Mon. Not. R. Astron. Soc. **271**, 693–705 (1994)

A dynamical study of the Ursa Minor dwarf spheroidal galaxy

J. C. Hargreaves,[1] G. Gilmore,[1] M. J. Irwin[2] and D. Carter[2]

[1] *Institute of Astronomy, Madingley Road, Cambridge CB3 0HA*
[2] *Royal Greenwich Observatory, Madingley Road, Cambridge CB3 0EZ*

Accepted 1994 July 20. Received 1994 July 11; in original form 1994 April 15

ABSTRACT

We have observed 46 giant stars in the Ursa Minor dwarf spheroidal (dSph) galaxy and obtained high-quality spectra for 35 of these. The velocity dispersion of the sample calculated by a maximum likelihood method is $7.5^{+1.0}_{-0.9}$ km s^{-1} and the mean velocity is -249.2 ± 1.5 km s^{-1}. There is evidence for rotation around the major axis: a straight line fit, equivalent to solid body rotation, gives a gradient of $-4.7^{+2.0}_{-2.2}$ km s^{-1} per 100 pc from the axis, where the positive distances are to the north-west of the major axis. This discovery adds evidence to the suggestion that Ursa Minor may be being tidally disrupted. If further work eliminates this possibility, then, assuming dynamical equilibrium, isotropy in the velocity dispersion (which is $6.7^{+0.9}_{-0.8}$ km s^{-1} when the rotation has been subtracted) and a negligible contribution from binary stars, the core mass-to-light ratio is 59^{+41}_{-25} $M_\odot/L_\odot$ and the total mass-to-light ratio is 40^{+29}_{-17} $M_\odot/L_\odot$, implying the presence of large quantities of dark matter.

Key words: galaxies: individual: Ursa Minor – galaxies: kinematics and dynamics – Local Group – dark matter.

1 INTRODUCTION

This paper presents the results from the most accurate velocity measurements available for stars in the Ursa Minor dwarf spheroidal (dSph) galaxy. These are used to calculate a velocity dispersion, to look for rotation around the axes, and to find the mean velocity for Ursa Minor.

Ursa Minor is the closest of the eight dSph galaxies known to be in orbit around the Milky Way. It is also distinguished by the detection of structure (Olszewski & Aaronson 1985): the luminosity contours show two clumps of stars along the major axis, separated by 16 arcmin (Irwin & Hatzidimitriou 1993). It is the most elongated of the dSph galaxies, with the major axis aligned along the polar ring, in the plane of the Magellanic Stream. In general, these galaxies contain a mixture of old and intermediate population stars and show no evidence of gas or recent star formation. In Ursa Minor, the population is dominated by old (15 Gyr) metal-poor stars (Olszewski & Aaronson 1985); this is illustrated by a strong blue horizontal branch in the colour–magnitude diagram (CMD). The dSph galaxies have similar total luminosity to most globular clusters (10^5–10^7 $L_\odot$), but their core radii are about an order of magnitude larger for the same luminosity.

Study of the kinematics of stars in both globular clusters and dSph galaxies by application of various simple models has been used to produce measurements for the mass-to-light ratios of these systems. The results for globular clusters are about 2 or 3 $M_\odot/L_\odot$, whereas those for the different dSph galaxies vary between 6 and 250 (Irwin & Hatzidimitriou, in preparation), and at face value imply that all the dSph galaxies are of similar mass but contain different proportions of luminous matter.

It is important to find the smallest scale on which large quantities of dark matter exist because it places constraints on what form that dark matter might take; for example, cold (or dissipative) dark matter can cluster on abitrarily short scales, while relativistic matter (e.g. neutrinos) cannot. Therefore, since dSph galaxies are the next largest scale objects after globular clusters, they are also the next largest scale on which to look for dark matter. However, a mass-to-light ratio of 250 for a dSph galaxy does seem inconsistent with the general trend of mass-to-light ratio compared with size in the rest of the Universe; for example, the value for the Milky Way Galaxy is only about 30, measured out to 80 kpc, and that for the Local Group is closer to 100 (Gilmore 1990). This and the wide range of measurements for the mass-to-light ratios of the different dSph galaxies leads to a question over whether the stellar kinematics are quite such simple indicators of the mass of these galaxies as is assumed by the simple models employed to date.

One possible complicating factor would be the presence of rotation, and quantifying rotation about either axis is important for several reasons: the axis about which the dSph rotates can give clues about possible triaxiality and anisotropy in the

velocity dispersion, and is a test for dissipation; rotation may also be related to possible tidal disruption by the Galaxy; and it is important to obtain the rotation, the rotation curve and the velocity dispersion profile for a complete mass determination of the system. In assessing possible rotation, it is important to allow for the effects of finite size, which, coupled with a high transverse motion, can mimic rotation.

The results from observations taken during the same observing runs as those discussed here but for the Sextans dSph galaxy have been presented in an earlier paper (Hargreaves et al. 1994). Since the reduction and analysis of the data were conducted in an identical manner for both sets of data, the discussion of the fine points of the procedures employed is not repeated here.

The rest of this paper is divided into the following sections. First, the observations and the reduction procedure are described. Next, the errors on the observations are discussed. Then the velocity dispersion calculation is described, the search for rotation explained and a value for the mass-to-light ratio obtained. Finally, other possible contributions to the velocity dispersion are discussed.

2 OBSERVATIONS, DATA REDUCTION AND ERROR ANALYSIS

2.1 Observations

The observations were made on the nights of 1991 May 4–7, 7–9 and 1992 April 26–27. All the observations were made using the William Herschel Telescope (WHT) in La Palma.

The spectral range observed was 8300–8750 Å, which is the region containing the prominent calcium II triplet absorption lines. We used the red arm of ISIS, the R1200R grating, a slit width of 1 arcsec with the slit aligned with the parallactic angle and an EEV 1280×1180 CCD as detector. The CCD was windowed to 400 pixels, which is about 2 arcmin, in the spatial direction. The resulting dispersion was about 0.35 Å per pixel, and the resolution measured from sky and arc lines was twice this. Arc lamp frames were taken before and after each stellar exposure using a CuNe lamp for the 1991 May run and CuAr and CuNe lamps for the others.

The stars observed were giant branch stars ranging in brightness from 15 to 18 mag in the *R* band. Observations were made of 60 Ursa Minor candidates of which 45 turned out to be members. Of the targets, 13 were kindly provided by Ed Olszewski (private communication). The proper motion membership probabilities of Cudworth, Olszewski & Schommer (1986), together with the proximity to the giant branch locus of our photographic CMD, were used to select 'inner' candidates, whilst the photographic CMD on its own was sufficient to select the 'outer' candidates. Good spectra were obtained for 35 members, with repeat observations for 21 of these, and nine had good spectra at two epochs. Out of these nine there was no firm evidence that any were binary stars. This topic is discussed further in Section 4.3.2 on the importance of binaries. Stars from the Sextans dSph galaxy were also observed during these runs, as well as during one other in 1991 December. The results of these observations have already been reported in an earlier paper (Hargreaves et al. 1994). The data for the stars observed in Ursa Minor and Sextans were considered together for definition of the internal and external errors, since the two data sets are of uniform precision.

In addition, four bright radial velocity standard stars (RV stars) were observed with integration times of only 5 s, one or two on each night of each run. These spectra provided an estimate of the random and systematic errors for high signal-to-noise ratio, short-exposure spectra. The random part of this error gave an estimate of the minimum random error for the Sextans data, although it appears that the RV stars may have greater systematic error due to slit centring problems. The details of this are discussed in Hargreaves et al. (1994). The RV stars were also used as a check on the data reduction procedure because their actual velocities were already known, and as a base to obtain the absolute mean velocity of Ursa Minor.

The coordinates of all the Ursa Minor member stars observed are shown in Table 1, and Table 2 contains a list of the coordinates of the observed non-members.

2.2 Data reduction

The processing of the CCD frames, data reduction and analysis were carried out in a very similar way to the Sextans data already published. A brief summary will suffice.

Preliminary processing of the CCD frames to remove bias and cosmic ray events was done, mostly at the telescope, using FIGARO routines. IRAF was then used to wavelength-calibrate, sky-subtract, and cross-correlate the data against the same template as was used for the Sextans data. The same line selection was used to throw out very poor lines from the spectra. The cross-correlation programme FXCOR produces a Tonry and Davis *R* value (Tonry & Davis 1979) for each

Table 1. Coordinates of the Ursa Minor stars. The centre of the Ursa Minor dSph galaxy is at $15^h8^m.4$, $67°25'$.

Star	RA 1950	DEC 1950	Star	RA 1950	DEC 1950
CUD1	15 08 52.6	67 28 25	EDO199	15 09 22.8	67 27 38
CUD9	15 08 53.3	67 24 18	EDO233	15 07 33.5	67 28 49
CUD34	15 10 02.4	67 24 55	EDO345	15 07 57.3	67 21 56
CUD37	15 10 07.8	67 24 08	EDON24	15 06 05.3	67 20 42
CUD87	15 09 41.9	67 27 11	EDON32	15 10 51.9	67 27 29
CUD96	15 08 38.8	67 29 05	EDON33	15 10 53.0	67 25 55
CUD107	15 09 03.8	67 28 58	EDON37	15 10 30.0	67 24 29
CUD122	15 09 56.3	67 30 23	EDON40	15 08 59.0	67 15 39
CUD132	15 08 52.7	67 31 32	EDON42	15 07 58.0	67 15 04
CUD189	15 08 05.6	67 24 35	EDOE	15 08 52.7	67 20 48
CUD267	15 08 30.3	67 28 28	EDOH	15 08 15.4	67 24 09
CUD234	15 07 33.9	67 28 31	UMJI1	15 10 03.1	67 38 55
CUD267	15 08 30.3	67 28 28	UMJI2	15 09 52.3	67 35 53
CUD297	15 07 49.9	67 21 30	UMJI5	15 10 45.0	67 33 49
CUD311	15 07 38.4	67 23 15	UMJI7	15 11 04.2	67 31 28
CUD366	15 08 13.3	67 21 32	UMJI8	15 11 13.7	67 30 50
CUD390	15 07 27.9	67 19 58	UMJI12	15 11 01.5	67 29 21
CUD397	15 08 04.2	67 20 07	UMJI13	15 10 10.7	67 27 57
CUD429	15 07 46.8	67 17 07	UMJI15	15 10 50.1	67 25 03
CUD459	15 09 15.3	67 23 36	UMJI18	15 09 18.0	67 23 22
CUD486	15 09 33.8	67 21 55	UMJI19	15 09 35.2	67 19 47
EDO26	15 09 32.9	67 24 09	UMJI20	15 07 17.5	67 18 43
EDO171	15 07 28.0	67 25 25	UMJI23	15 05 42.2	67 15 34

Notes. The stars labelled CUD are those listed by Cudworth et al. (1986) as high-probability members from their derived proper motions, while the EDO stars are those found by Olszewski (1991, private communication) and the UMJI stars are new members found purely using their spatial location and proximity to the giant-branch locus on a photographic CMD.

Table 2. Coordinates of the non-members found.

Star	RA 1950	DEC 1950
CUD442	15 07 55.0	67 15 53
CUD508	15 09 39.6	67 17 11
UMJI3	15 07 15.6	67 34 10
UMJI4	15 09 46.8	67 43 39
UMJI6	15 10 24.1	67 32 17
UMJI9	15 09 10.1	67 30 36
UMJI11	15 06 26.1	67 29 14
UMJI14	15 09 00.5	67 26 54
UMJI16	15 06 42.9	67 24 27
UMJI17	15 06 48.3	67 24 21
UMJI21	15 06 23.0	67 18 24
UMJI22	15 08 56.8	67 16 57
UMJI25	15 09 04.8	67 13 56
UMJI26	15 09 20.0	67 13 43
UMJI27	15 06 22.3	67 13 18

Notes. The stars labelled UMJI are those stars we observed for the first time that turned out not to be members. The two CUD stars were those identified as high-probability members from their proper motions by Cudworth et al. (1986). CUD442 has the colours and kinematics of a halo K-giant.

correlation, and it was this parameter that was used to produce a cut-off value below which the results were considered too inaccurate and therefore discarded. In the case of star UMJI12, it was possible to combine the two spectra with R value below the cut-off to produce one high-quality spectrum.

2.3 Errors in the velocities

The errors on the Ursa Minor data were calculated in the same way as for the Sextans data, using the differences in the velocities obtained for repeat measurements. The cut-off value for R (R_{cut}) was found by comparing these differences in velocity with the R values of the measurements. There are considerably fewer repeat measurements per star for the Ursa Minor observations as compared with those in Sextans, so the error information for the two data sets was combined, and the result is the appropriate measuring error for Ursa Minor. The repeat measurements for the possible binary, star 8, in the Sextans data (Hargreaves et al. 1994) were removed from this data set.

The mean for each star was calculated, sigma clipping the most extreme velocities. This is $\overline{V}_{ex}$ in Table 3 and the velocities that were clipped out of the average are marked by an asterisk. The difference of each measurement from this mean value is ΔV_{ex} in the same table. Fig. 1 is the σ_{ex} versus R diagram for the combined data set, where σ_{ex} is the standard deviation of the values of ΔV_{ex} at each value of R. Fig. 1 shows clearly how the value of σ_{ex} rises with decreasing R

Table 3. The velocities and Tonry and Davis R values for the Ursa Minor observations. (The columns are explained in the table footnotes and the text.)

Star	Date	R	V_t km s^{-1}	$\overline{V}_{ex}$ km s^{-1}	ΔV_{ex} km s^{-1}	$\overline{V}_{7.5}$ km s^{-1}	$\Delta V_{7.5}$ km s^{-1}
CUD1	M91	9.78	0.6	4.1	-3.6	4.1	-3.6
	A92-1	11.50	7.4		3.3		3.3
	A92-1	12.14	4.4		0.3		0.3
CUD9	M91	4.35	2.6	2.6	—	—	—
CUD34	M91	9.33	3.8	3.8	—	3.8	—
CUD37	M91	4.61	4.5	0.9	3.5	—	—
	M91	9.24	-2.6		-3.5	-2.6	—
CUD87	M91	17.79	-5.0	-5.0	—	-5.0	—
CUD96	M91	11.46	-4.4	*	-4.6	-1.4	-3.1
	M91	9.26	-0.5	0.2	-0.7		0.8
	A92-1	8.13	0.9		0.7		2.2
CUD107	M91	11.48	-4.5	-4.5	—	-4.5	—
CUD122	A92-1	8.74	0.6	0.6	—	0.6	—
CUD132	M91	7.68	-2.8	-2.8	—	-2.8	—
CUD189	M91	10.83	-0.6	-0.6	—	-0.6	—
CUD234	M91	5.19	-9.8	-9.8	—	—	—
CUD267	M91	6.66	-0.9	-0.9	—	—	—
CUD297	M91	15.56	11.6	9.2	2.4	9.2	2.4
	A92-2	14.19	6.8		-2.4	9.2	-2.4
CUD311	M91	5.00	-11.6	-11.6	—	—	—
CUD366	M91	6.62	-4.1	-8.3	4.2	—	—
	M91	8.23	-12.4		-4.2	-12.4	—
CUD390	M91	4.56	-35.4	-35.4	—	—	—
CUD397	M91	5.98	17.5	17.5	—	—	—
CUD429	A92-1	3.21	16.8	16.8	—	—	—
CUD442	M91	6.67	87.3	(81.7)	5.7	—	—
	A92-1	5.43	76.0		-5.7	—	—
CUD459	M91	7.44	-7.8		—	—	—
CUD486	M91	6.11	2.8		—	—	—
	A92-1	3.95	—	—	—	—	—
EDO26	M91	18.04	10.9	*	-2.5	12.5	-1.6
	A92-1	11.78	13.7	13.3	0.4		1.2
	A92-2	12.67	12.9		-0.4		0.4
EDO171	M91	13.88	-13.1		0.7	-13.8	0.7
	A92-1	10.89	-14.6	-13.8	-0.7		-0.7
	A92-2	6.70	-7.8	*	6.0	—	—
EDO199	M91	16.47	-3.1		0.1	-2.7	-0.5
	A92-1	13.57	-3.4	-3.3	-0.1		-0.7
	A92-2	12.82	-1.5	*	1.8		1.2
EDO233	M91	12.52	-17.0	-17.0	-0.1	-17.9	0.8
	A92-1	13.17	-19.7	*	-2.7		-1.8
	A92-2	30.24	-16.9		0.1		1.0

Table 3 – *continued*

Star	Date	R	V_t km s^{-1}	$\overline{V}_{ex}$ km s^{-1}	ΔV_{ex} km s^{-1}	$\overline{V}_{7.5}$ km s^{-1}	$\Delta V_{7.5}$ km s^{-1}
EDO345	M91	15.44	-3.2	-3.4	0.2	-3.4	0.2
	M91	10.48	-3.6		-0.2		-0.2
EDON24	M91	19.83	-6.6	-6.6	—	-6.6	—
EDON32	M91	7.42	-4.4	-4.4	—		—
EDON33	M91	9.80	1.7	-1.5	3.2	-1.5	3.2
	A92-2	14.02	-4.7		-3.2		-3.2
EDON37	M91	13.30	2.2	3.0	-0.8	3.0	-0.8
	M91	9.79	3.8		0.8		0.8
EDON40	M91	9.13	25.0		5.7		6.9
	M91	4.08	24.0		-4.7	—	—
	M91	8.30	14.2	19.3	-5.2	18.2	-4.0
	A92-1	6.80	14.3		-5.0		-3.9
	A92-2	9.43	19.1		-0.2		1.0
EDON42	M91	6.91	7.9	6.6	1.3	—	—
	M91	11.11	5.4		-1.3	5.4	—
EDONE	M91	7.68	-12.9	-12.9	—	-12.9	—
EDONH	M91	14.39	3.3	3.4	—	3.3	—
UMJI1	A92-1	12.39	-1.0		0.2	-3.0	2.1
	A92-1	8.88	-7.3	*	-4.3		-4.3
	A92-2	14.62	-1.4	-1.2	-0.2		1.6
	A92-2	7.67	-2.5	*	-1.3		0.6
UMJI2	A92-1	12.39	-13.9	-12.8	-1.1	-12.8	-1.1
	A92-2	21.53	-11.7		1.1		1.1
UMJI5	A92-1	14.70	10.0	8.1	1.9	8.1	1.9
	A92-2	9.24	6.1		-1.9		-1.9
UMJI7	A92-1	7.60	-2.7	-2.8	0.1	-2.8	0.1
	A92-2	9.90	-2.9		-0.1		-0.1
UMJI8	A92-1	10.06	1.9	0.5	1.4	0.5	1.4
	A92-2	13.98	-1.0		-1.4		-1.4
UMJI12	A92-1	6.47	5.0	-0.2	5.2	—	—
	A92-2	6.10	-5.4		-5.2	—	—
	comb	8.40	0.8	—	—	0.8	—
UMJI13	A92-1	9.94	-7.9	-6.1	-1.8	-6.1	-1.8
	A92-2	10.74	-4.3		1.8		1.8
UMJI15	A92-1	10.90	-6.6	-6.3	-0.4	-6.3	-0.4
	A92-2	8.39	-5.9		0.4		0.4
UMJI18	A92-1	8.26	-4.4	-4.1	-0.3	-4.1	-0.3
	A92-2	10.44	-3.8		0.3		0.3
UMJI19	A92-1	10.27	0.2	0.4	-0.2	0.4	-0.2
	A92-2	9.34	0.6		0.2		0.2
UMJI20	A92-1	5.24	9.3	7.6	1.8	—	—
	A92-2	12.18	5.8		-1.8	5.8	—
UMJI23	A92-1	9.50	-10.8	-8.6	-2.3	-8.6	-2.9
	A92-2	10.79	-6.3		2.3		2.9

value, a suitable cut-off value being somewhere between 7 and 8.

For a variety of values of R_{cut}, an error distribution was created from the differences of the velocities obtained from individual observations for a star compared with the real mean velocity of that star. The standard deviation of this distribution was the appropriate error on an individual observation.

The widths of the error distributions for R_{cut} values of 0, 7, 7.5 and 8 were 5.5 ± 0.3, 2.3 ± 0.2, $2.0^{+0.1}_{-0.2}$ and 2.0 ± 0.2 km s^{-1}, respectively. If the width of the distribution is denoted by σ_{err}, then the error quoted here is such that the variance on σ^2_{err} is $2\sigma^2_{err}/N$. Komolgorov–Smirnov (K–S) tests to compare the actual error distributions with Gaussians gave probabilities that implied consistency, except for the case for an R_{cut} value of 0, where the probability was 0.003. The failure of the K–S test was expected for this case because the wide range of R values for the velocities made a single value for the measuring error inappropriate. Table 4 contains all the error results for the different cut-off values.

The cut-off value used for the rest of the analysis was 7.5, since this was the value at which the error first dropped to a low value whilst still retaining a large number of the stars. Fig. 2 shows the error distribution, for the Ursa Minor and Sextans data, and the fitted Gaussian for an R_{cut} value of 7.5.

3 RESULTS

3.1 The velocity dispersion calculation

The observations that produced R values above the threshold were used to calculate a mean velocity for each star. The width of the distribution of these velocities defined the velocity dispersion (σ_{obs}) of Ursa Minor. An unweighted Gaussian fit to the data was made for comparison with the error-weighted fit. The results reported in the text are those for an R_{cut} value of 7.5. Table 4 contains the details of all the results for different values of R_{cut}.

The velocity dispersion obtained by fitting a Gaussian to the unweighted distribution was $7.7^{+0.9}_{-1.0}$ km s^{-1}. The variance of σ^2_{obs} is $2\sigma^4_{obs}/N$, so this is the error quoted. This dispersion has not had the contribution due to measuring errors removed. The inclusion of this, as in equation (22) of

Notes. Date: M91, A92-1 and A92-2 are abbreviations for the 1991 May and 1992 April runs, A92-1 being the run at the start of April and A92-2 the one at the end.
V_t: this is the heliocentrically corrected velocity with respect to the template.
R is the Tonry & Davis R value.
$\overline{V}_{ex}$: this is the average for each star of all the values of V_t excluding those that caused a change in the mean of more than 2.5 standard deviations. The excluded stars are marked by an asterisk.
CUD442 is not a member of Ursa Minor: it is probably a halo star, but, since we happen to have two observations of it, its errors were included in the analysis.
$\overline{V}_7$: this is the average velocity for a star where data that produced a correlation with $R < 7$ are not included, and $\Delta V_7 = (V_t - \overline{V}_7)$.
For UMJI12, the combination of the two spectra produced a spectrum with an R value above the threshold. The combined spectrum is marked by 'comb'.
The observations not included at the cut-off are marked by a dash.

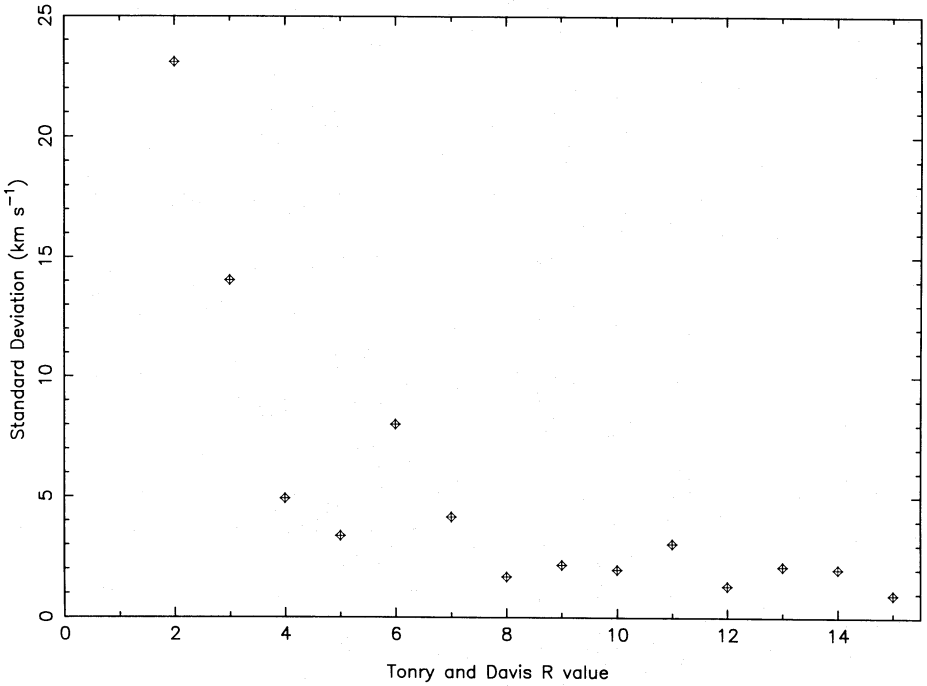

Figure 1. Standard deviation of the variations of the repeat velocities versus the Tonry & Davis R value: the calculation of the standard deviations is explained in the text. The steep increase in the standard deviation with decreasing R at low R is as expected for an accuracy versus R diagram. The deduced cut-off value for R is between 7 and 8.

appendix B in Hargreaves et al. (1994), gave a corrected velocity dispersion of $7.6^{+0.9}_{-1.0}$ km s^{-1}.

A better way to calculate the results is to weight each velocity by its error in some way. In Hargreaves et al. (1994), we compared the method commonly used (Armandroff & Da Costa 1986) with the use of a maximum likelihood estimator, and concluded that the maximum likelihood estimator was the more appropriate for this situation. The resulting definitions for the mean velocity and velocity dispersion are

$$\hat{\bar{v}} = \frac{\sum_i w_i v_i}{\sum_i w_i}, \tag{1}$$

$$\hat{\sigma}^2_{\rm obs} = \frac{\sum[(v_i - \bar{v})^2 - \sigma_i^2]\, w_i^2}{\sum_i w_i^2}, \tag{2}$$

where v_i is the velocity of each star and σ_i is the error on each star. The equations were solved by an iterative procedure whereby $w_i = 1/(\sigma_i^2 + \sigma^2_{\rm obs})$ was updated on each iteration.

With the use of the maximum likelihood method, the velocity dispersion for an $R_{\rm cut}$ value of 7.5 was $7.5^{+1.0}_{-0.9}$ km s^{-1}. For a sample where the velocity dispersion is considerably larger than the measuring errors, it is expected that this result will be similar to the unweighted calculation, as explained in the appendix of Hargreaves et al. It can be seen, referring to Table 4, that this is indeed the case for our results. Fig. 3 shows the velocity distribution for an $R_{\rm cut}$ value of 7.5, with the fitted Gaussian derived by the maximum likelihood method.

Velocity measurements in Ursa Minor have been made over several years by Olszewski and co-workers, the most recent published value for the velocity dispersion being 12.0 ± 2.4 km s^{-1} (Mateo 1994), a value inconsistent with our result.

3.2 Rotation and the mean velocity

Ursa Minor is elliptical in shape, with an ellipticity of 0.56. This flattening could be caused by rotation of the dSph galaxy, anisotropy in its velocity dispersion, strong tidal interaction with the Milky Way, or some combination of the three. Rotation would artificially increase the observed velocity dispersion providing that the rotation was not in the plane of the sky. Detection of rotation is important for other reasons: the rotation curve and velocity dispersion are both required to determine correctly the mass of the system; and if the galaxy is exerting a large tidal torque, disrupting the dSph, it would be expected to generate rotation. Determination of the axis about which the dSph rotates is a test for triaxiality of the dSph galaxy, and for dissipation.

Before looking for rotation, the velocities in Ursa Minor were corrected to a Galactocentric system to eliminate the differential heliocentric corrections over an object of large finite extent. The average change in the velocity of each star caused by this correction was 0.2 km s^{-1}. Then, to check for any sign of rotation, the distances of each star from the morphological major and minor axes were calculated, and straight lines were fitted to the velocity–distance plots: a straight line is the expected form of the rotation curve for solid body rotation. The gradient of the fit for rotation about the major axis was a factor of 10 greater than for that about the minor axis (-4.4 km s^{-1} per 100 pc compared with

Table 4. Widths of the error distributions and the velocity dispersions calculated for different value of R_{cut}.

Distribution	$\bar{v}$ km s^{-1}	σ km s^{-1}	Error km s^{-1}	Prob	N
Ursa Minor and Sextans error calculation					
all R	0.1	5.5	$\pm^{0.3}_{0.3}$	0.003	138
R ≥ 7	−0.01	2.3	$\pm^{0.2}_{0.2}$	0.48	92
R ≥ 7.5	3x10^{-4}	2.0	$\pm^{0.1}_{0.2}$	0.60	87
R ≥ 8	2x10^{-4}	2.0	$\pm^{0.2}_{0.2}$	0.71	84
Ursa Minor velocity dispersion					
Unweighted calculation					
all R	-1.6	9.6	$\pm^{1.0}_{1.1}$	0.79	45
R ≥ 7	-1.8	7.6	$\pm^{0.8}_{0.9}$	0.90	37
R ≥ 7.5	-1.6	7.7	$\pm^{0.9}_{1.0}$	0.92	35
R ≥ 8	-1.2	7.7	$\pm^{0.9}_{1.0}$	0.93	33
Unweighted calculation (measuring errors included)					
all R	-1.6	8.7	$\pm^{0.9}_{1.0}$	0.96	45
R ≥ 7	-1.8	7.4	$\pm^{0.8}_{0.9}$	0.92	37
R ≥ 7.5	-1.6	7.6	$\pm^{0.9}_{1.0}$	0.93	35
R ≥ 8	-1.2	7.5	$\pm^{0.9}_{1.0}$	0.94	33
Maximum Likelihood calculation					
all R	-1.5	8.3	$\pm^{1.2}_{1.0}$	0.97	45
R ≥ 7	-1.8	7.3	$\pm^{1.0}_{0.8}$	0.91	37
R ≥ 7.5	-1.5	7.5	$\pm^{1.1}_{0.9}$	0.94	35
R ≥ 8	-1.2	7.5	$\pm^{1.0}_{0.9}$	0.94	33
Maximum Likelihood calculation for velocities minus rotation					
R ≥ 7.5	-0.7	6.7	$\pm^{0.9}_{0.8}$	0.91	35

Notes. The value $\bar{v}$ is the average value calculated by the fit to the distribution.
The value of σ is the width of the distribution; so, in the case of the error distribution, it is the value of the error and in the case of the velocity dispersion calculation it is the velocity dispersion.
Error is the error in the value of σ calculated as described in the text.
N is the number of stars in the distribution.
The value 'Prob' is the probability obtained by a K–S test comparing a Gaussian distribution with the calculated width and average to the actual distribution of data.
The differences between the different calculations (weighted and unweighted) are described in the velocity dispersion section.

−0.1 km s^{-1} per 100 pc), so more investigation was required.

Our data set is one of the many possible sets of data for Ursa Minor. The most complete way to calculate the significance of the apparent rotation would be to simulate data sets by assuming values for the intrinsic velocity dispersion and rotation, and to see how likely it is that we would obtain apparent rotation as in our original data set. Bootstrap re-sampling is a simple and convenient way to make a similar calculation without having to do a full Monte Carlo simulation.

Bootstrap re-sampling involves taking data points at random, with replacement, from the original data set, in order to build another sample data set. The analysis is repeated on this new data set as for the original, and the parameters obtained are recorded. This is repeated many times, the median of the distribution of each parameter now being the best estimate of that parameter and the width of the distribution being the error. In our case, we took 1000 samplings and found the values of the intercept and gradient for a straight line fitted to the data. The results were consistent with rotation about the major axis. The disadvantage of this method is that the 'new' samples are not independent of the original.

Fisher randomization (Fisher 1958) is, in many ways, a superior procedure, since it uses all the data points in such a way as to create independent samples. The velocities from our data set were randomly paired with the distances from the rotation axis to produce many new data sets. The number of times that the straight line fit to the new data set produces a gradient larger than that obtained from our original set was calculated. The question answered here is how likely it is that the data with a velocity dispersion of $7.5^{+1.0}_{-0.9}$ km s^{-1} and no rotation could produce apparent rotation of the magnitude we observed. For rotation around the major axis, the answer was 0.58 per cent, and around the minor axis it was 45.97 per cent, which implies a 3σ effect around the major axis, but no significant rotation around the minor axis.

The axis of greatest rotation was found by fitting solid body rotation curves to the distance–velocity information around every possible axis at 1° intervals. The position angle giving the greatest apparent rotation was 58°, in agreement with the morphological major axis calculated by Irwin & Hatzidimitriou (in preparation), which was 53°±5°. The effect of changing the position angle for the rotation by about 20° was to produce a significant decrease, of about 30 per cent, in the magnitude of the apparent rotation. Whilst this is not the error on the position angle of greatest rotation, because one will always see a component of the rotation about any other axis that is not perpendicular to the true axis, it does give some idea of the rate of change of rotation with position angle. The following values for our estimate of the rotation effect are the median values of the intercept and gradient produced by taking a position angle of 58° and applying the bootstrapping procedure 1000 times.

Around the major axis, the intercept $= -2.5 \pm 1.5$ km s^{-1} and the gradient $= -4.7^{+2.0}_{-2.2}$ km s^{-1} per 100 pc. Here the positive distances are on the north-western side of the major axis. Around the minor axis, the intercept $= -1.4^{+2.3}_{-2.0}$ km s^{-1} and the gradient $= 0.1^{+0.8}_{-1.1}$ km s^{-1} per 100 pc. The positive distances are on the north-eastern side of the minor axis.

For both these cases, the intercept is with respect to an arbitrary value which is actually the velocity with respect to the template plus 470 km s^{-1}. The errors quoted are the 68 per cent level of the distribution for each variable, holding the other one fixed. The goodness of fit of the lines is, of course, very poor since the velocity dispersion about the mean rotation is large ($\chi^2 \sim 840$ for 35 stars), but it does appear that there is a real indication of rotation about the major axis at the 99.5 per cent level of significance from the Fisher randomization test. Figs 4 and 5 show the velocity–distance data for the major and minor axes, the fitted lines being those with the parameters quoted above. For the rotation that we have observed to be an artefact produced by our line of sight and the transverse motion of the dSph galaxy, Ursa Minor would have to be travelling at more than 2500 km s^{-1} in an orbit in the direction of its minor axis. It is

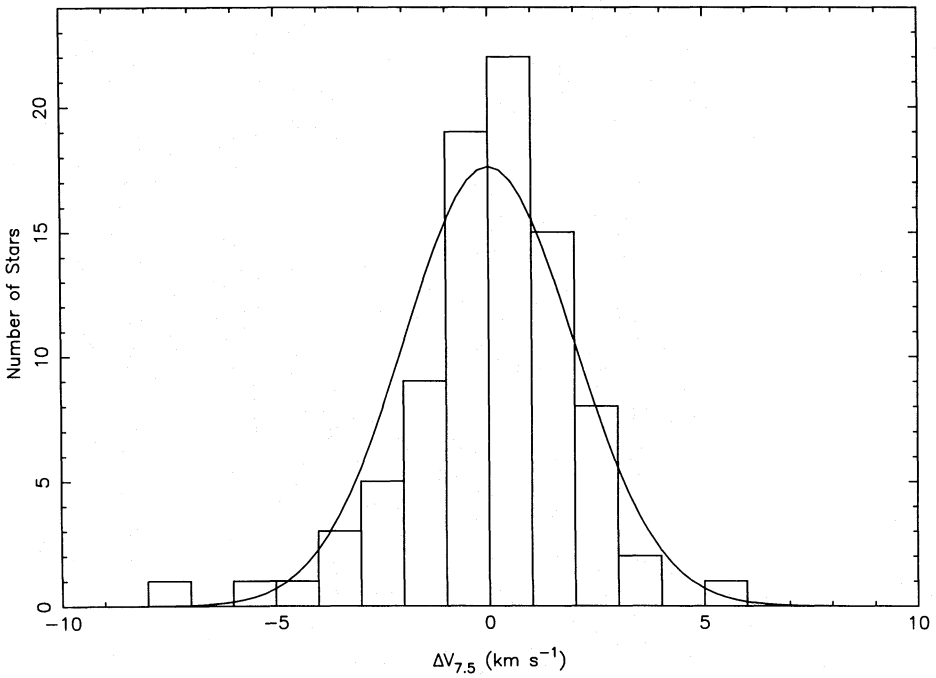

Figure 2. The Gaussian fit to the error distribution of the Ursa Minor stars for an R_{cut} value of 7.5 with width 2.0 km s^{-1}. The K–S test of this fit produced a probability of 0.60.

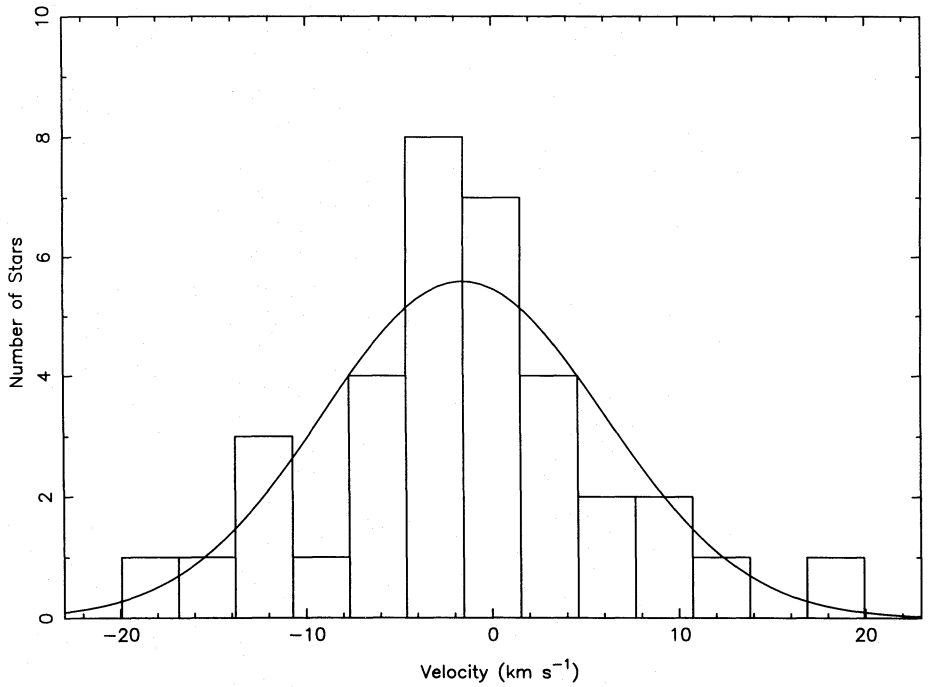

Figure 3. The velocity distribution of the Ursa Minor dSph galaxy with an R_{cut} value of 7.5. There are 35 stars in the sample and the Gaussian shown is that produced by the maximum likelihood calculation. The velocity dispersion is 7.5 km s^{-1} and the average velocity −1.5 km s^{-1} with respect to the template plus 470 km s^{-1}.

highly unlikely that the dSph galaxy would have a transverse velocity this large, as the expected transverse velocity for a bound orbit is more likely to be about 300 km s^{-1}. Furthermore, the evidence points towards the orbit being in the direction of the major axis, a point that is discussed in Section 4.3.3 of this paper.

The presence of rotation lowers the value of the velocity dispersion, as the rotation curve has to be subtracted from the velocities. In our case, this leads to a velocity dispersion, calculated using a maximum likelihood method, of $6.7^{+0.9}_{-0.8}$ km s^{-1}. Comparing this with the value without correction for rotation ($7.5^{+1.0}_{-0.9}$ km s^{-1}), it is apparent that both the derived

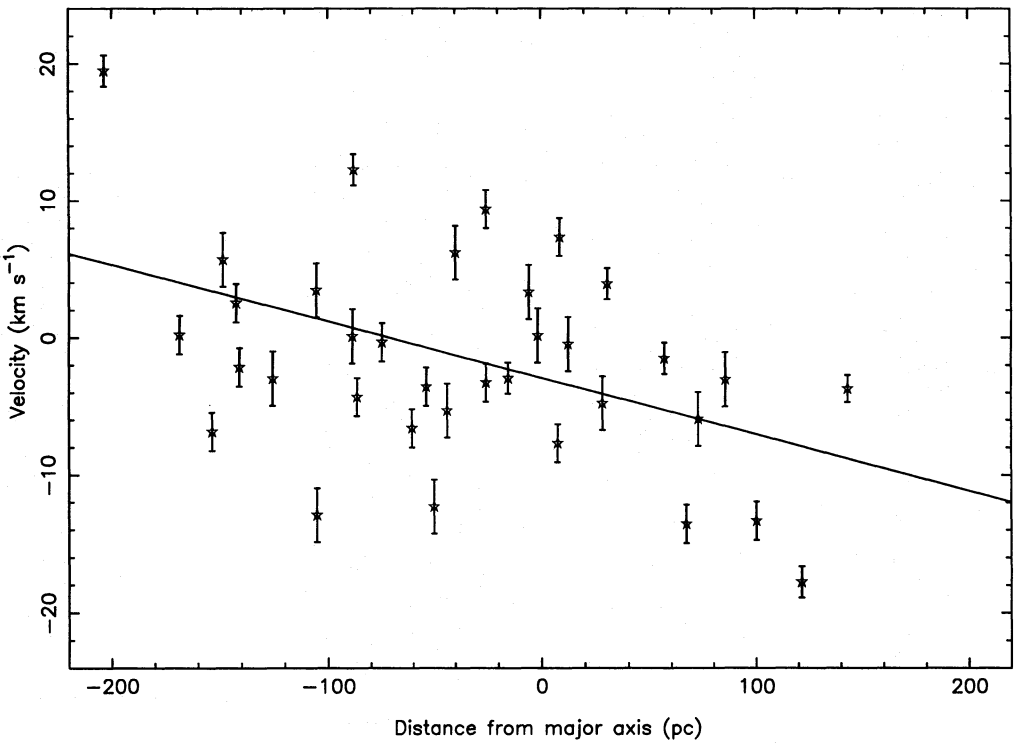

Figure 4. The rotation around the major axis of Ursa Minor at a position angle of 58°. The line is the median line from the bootstrapping method, with a gradient of -4.7 km s^{-1} per 100 pc and an intercept at -2.5 km s^{-1}.

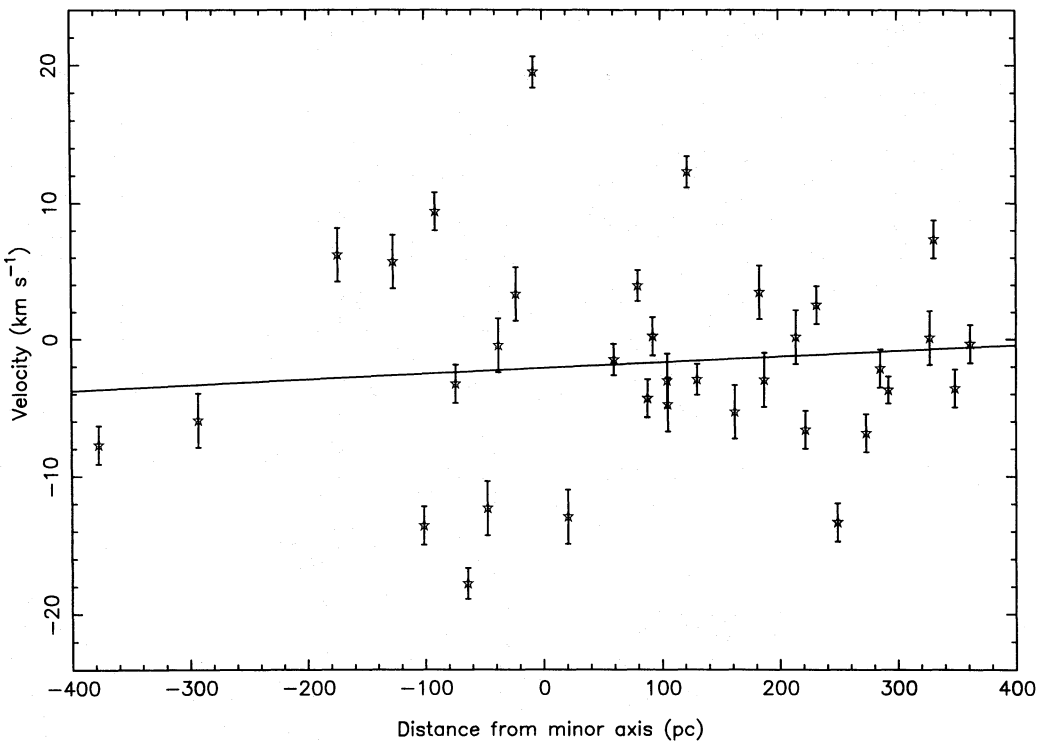

Figure 5. There was negligible rotation around the minor axis of Ursa Minor. The line is the median line from the bootstrapping method, with a gradient of 0.1 km s^{-1} per 100 pc and an intercept at -1.4 km s^{-1} at a position angles of 58°.

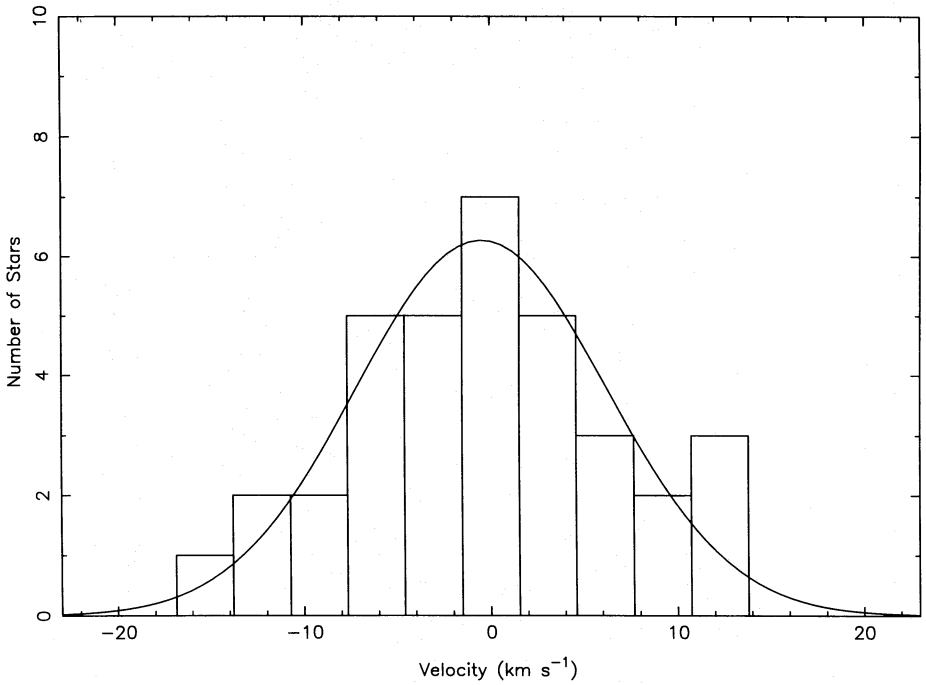

Figure 6. The velocity distribution of the Ursa Minor dSph galaxy with an R_{cut} value of 7.5 with the effect from rotation subtracted. The velocity dispersion calculated by the maximum likelihood method is 6.7 km s^{-1} and the average velocity -0.7 km s^{-1}.

Table 5. How velocity dispersion varies with radius.

Radius range pc	Average radius pc	No. in bin	Velocity dispersion. Straight data km s^{-1}	Rotation subtracted km s^{-1}
16-67	49	7	$6.0\pm^{1.6}_{2.1}$	$6.7\pm^{1.7}_{2.3}$
70-104	89	7	$9.3\pm^{2.3}_{3.0}$	$8.0\pm^{2.0}_{2.6}$
104-152	130	7	$7.3\pm^{1.8}_{2.4}$	$5.8\pm^{1.5}_{2.0}$
158-227	190	7	$4.7\pm^{1.2}_{1.7}$	$4.1\pm^{1.1}_{1.6}$
235-290	261	7	$4.5\pm^{1.2}_{1.6}$	$5.3\pm^{1.3}_{1.8}$

dispersion and the 1σ error range have been reduced. The difference in the derived velocity dispersion using velocities corrected to Galactocentric coordinates and uncorrected was negligible. Fig. 6 shows the fit of the new velocity dispersion to the velocity distribution corrected for rotation. At the last measured distance on the minor axis, of close to 200 pc, the solid body rotation curve produces a maximum rotational velocity of 8.2 km s^{-1}. The rotational velocity divided by the velocity dispersion is $8.2/6.7 = 1.2$, implying considerable support in the galaxy from rotation as well as from the velocity dispersion. This value is consistent with a triaxial galaxy with no anisotropy, rather than with a prolate galaxy rotation end over end.

The discovery of rotation in Ursa Minor is of particular interest when placed in the context of the other dSph galaxies. For example, Hargreaves et al. (1994) found no sign of rotation about either axis of the Sextans dSph galaxy, whereas Paltoglou & Freeman (1987) claim a rotational velocity of 3.5 ± 2.5 km s^{-1} about the minor axis of Fornax at about one core radius, but this is not confirmed by Mateo et al. (1991).

The other result obtained was that for the systematic velocity of the Ursa Minor dSph galaxy. From the RV standard stars, the velocity of the template was found to be 223.3 km s^{-1}. The results quoted in Tables 3 and 4 are those relative to the template plus 470 km s^{-1}. These data gave a median intercept on the rotation curve of -2.5 ± 1.5 km s^{-1}. Therefore the velocity of Ursa Minor was $223.3 - 470 - 2.5 = -249.2 \pm 1.5$ km s^{-1}. This value is in agreement with the value of -249 ± 1 km s^{-1} given in Zaritsky et al. (1989).

4 ANALYSIS

4.1 Variation of velocity dispersion with radius

For a King model (King 1962, 1966) of a stellar system without an extended massive halo, it is expected that the velocity dispersion will decrease with distance from the centre of the galaxy (e.g. Hargreaves et al. 1994). Table 5 shows how the velocity dispersion varies with distance for our results, the 'radius' being the geometric mean radius, since Ursa Minor is elliptical in shape (Irwin & Hatzidimitriou, in preparation). The two columns of values displayed contain the results for the data with an R_{cut} value of 7.5 and those for these same data with the effect of rotation subtracted. The dispersions and errors here were calculated as before, using the maximum likelihood method. The velocity dispersion shows some sign of decrease at radii greater than the core radius of 196 pc: Fig. 7 shows the results for the data corrected for the effect of rotation. Within the errors, the variation of the velocity dispersion for the data with and without rotation subtracted are consistent with the King model with concentration, $c = 0.51$, derived for Ursa Minor by Irwin & Hatzi-

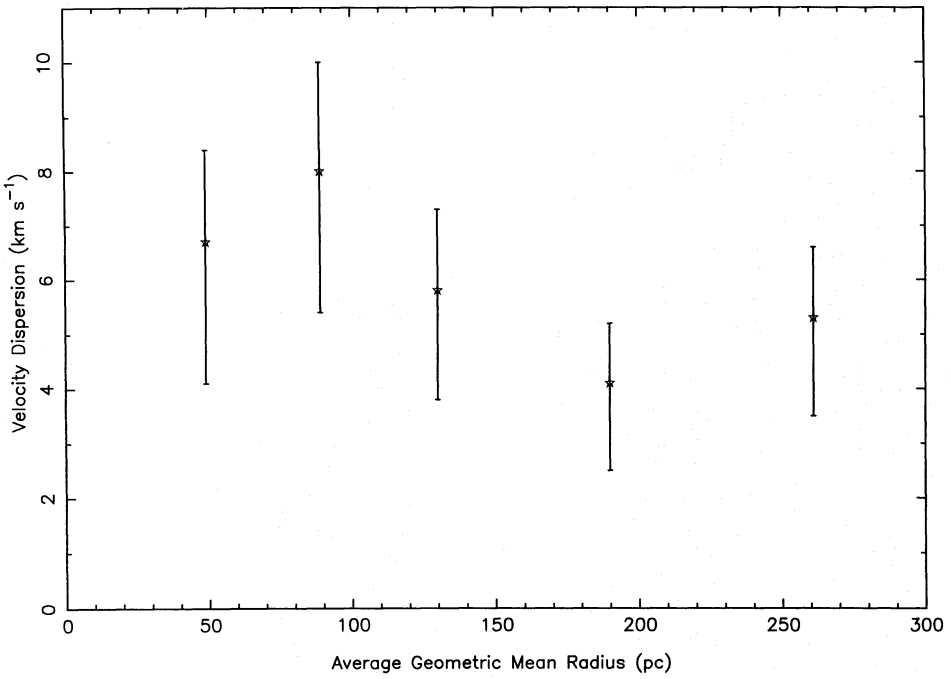

Figure 7. The variation of the velocity dispersion with distance from the centre of Ursa Minor. The data are from Table 5 and have been corrected for the effect of rotation.

dimitrou (in preparation). We emphasize that the combination of an apparent rotation and a decrease in velocity dispersion with distance in Ursa Minor means that a detailed dynamical analysis of this Galactic dSph is in principle possible. Velocities for stars further from the centre of Ursa Minor are required to extend this result.

4.2 Mass-to-light ratios

The background to the methods used to calculate the mass-to-light ratio are given in Hargreaves et al. (1994). The resulting equations for the core and total mass-to-light ratios, hereafter called the core-fitting method and Illingworth's method, respectively, are

$$\frac{\rho_0}{I_0} = \eta \frac{333\sigma_0^2}{r_{\rm hb} S_0}, \tag{3}$$

and

$$\frac{M_{\rm tot}}{L_{\rm tot}} = \frac{166.5 r_{\rm c} \mu}{\beta L_{\rm tot}}, \tag{4}$$

where η and μ are parameters given by the particular King model; σ_0^2 and $1/\beta$ are the observed square velocity dispersions, $\sigma_{\rm obs}^2$, adjusted according to the King model and average radius of the stars observed I_0 and $L_{\rm tot}$ are the central surface brightness and total luminosity of the dSph; and $r_{\rm c}$ and $r_{\rm hb}$ are the core and half-brightness radii, respectively. Illingworth's method is far more model-sensitive because η is always close to unity but μ varies considerably with small changes in the concentration of the King model.

The King model with $c = 0.51$ has $W_0 = 2.4$, and the parameters $\eta = 0.96$ and $\mu = 2.7$. Fig. 8 shows the photometric data fitted by this King model (solid line) and the best-fitting exponential profile (dashed line).

Irwin & Hatzidimitriou also calculated the following parameters for the dSph galaxy:

$r_{\rm c} = 196 \pm 24$ pc,

$r_{\rm hb} = 150 \pm 18$ pc,

$r_{\rm t} = 628 \pm 74$ pc,

$M_V = -8.7 \pm 0.5$,

$L_{{\rm tot},V} = (2.5^{+1.6}_{-0.9}) \times 10^5\ {\rm L}_\odot$,

$S_{0,V} = 2.0^{+1.2}_{-0.8}\ {\rm L}_\odot\ {\rm pc}^{-2}$.

All the distances quoted here are geometric mean distances. The average distance from the centre of the galaxy of our observations was 144 pc, which is $0.73 r_{\rm c}$, leading to $\sigma_0 = \sigma_{\rm obs}/0.90$ and $1/\beta = \sigma_{\rm obs}^2/0.54^2$, where $\sigma_{\rm obs}$ is the observed velocity dispersion. The velocity dispersion for the data with an $R_{\rm cut}$ of 7, with the effect of our derived rotation subtracted, was $\sigma_{\rm obs} = 6.7^{+0.9}_{-0.8}$ km s^{-1}. The mass-to-light ratios were calculated by simulating a distribution assuming Gaussian errors and taking the median value. The result for the core mass-to-light ratio was $\rho_0/I_{0,V} = 59^{+41}_{-25}$. Similarly, the total mass-to-light ratio was $M_{\rm tot}/L_{{\rm tot},V} = 40^{+29}_{-17}$. The errors quoted here include those due to the half-brightness and core radii, the luminosity and the velocity dispersion, and they are taken at the 68 per cent level of the derived distribution, the luminosity error contributing more than half the total error. For the velocity data without rotation subtracted, the results were $\rho_0/I_{0,V} = 74^{+51}_{-31}$ and $M_{\rm tot}/L_{{\rm tot},V} = 50^{+36}_{-22}$. Our values for the mass-to-light ratios are considerably less than the values

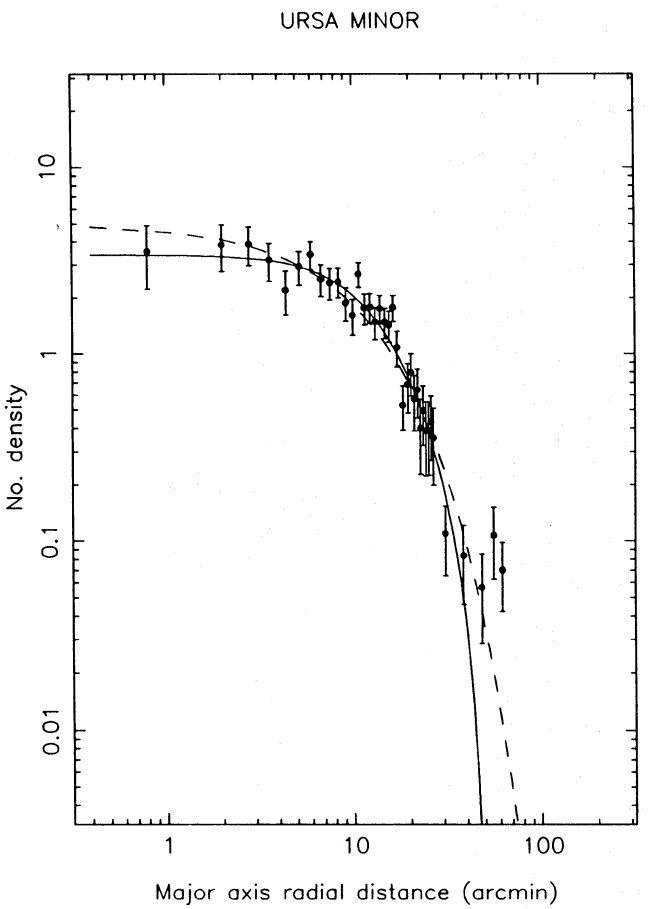

Figure 8. The best King model fitted to the Ursa Minor dSph galaxy (by Irwin & Hatzidimitriou, in preparation, from the APM results) with a concentration of 0.51. The dashed line is an exponential fit. 1 arcmin is equivalent to 18.6 parsec at the distance of Ursa Minor (64 kpc).

previously published for Ursa Minor, which have been between 80 and 150 (Aaronson & Olszewski 1987; Pryor 1991). The differences are due mostly to our lower velocity dispersion.

For the mass-to-light ratio to be 3, σ_{obs} would need to be about 2 km s^{-1}. This is well outside the 99.9 per cent confidence level value of 4.3 km s^{-1} from the maximum likelihood calculation. Such a small dispersion would only just be detectable because the dispersion caused by our errors alone is 1.5 km s^{-1}.

4.3 Other possible explanations of the velocity dispersion

4.3.1 Anisotropy of the velocity dispersion

The models used to calculate the mass-to-light ratio assumed isotropy in the velocity dispersion. That is,

$$\sigma^2_{total} = \sigma^2_{los} + \sigma^2_{\theta} + \sigma^2_{\phi} = 3\sigma^2_{los}, \quad (5)$$

where σ_{los} is the line-of-sight velocity dispersion, and σ_{θ} and σ_{ϕ} are the dispersions that would be seen along the other two perpendicular directions. So, the maximum effect that anisotropy could have on the mass-to-light ratio is a factor of 3 (the calculated mass-to-light ratio would be a factor of 3 higher than the true answer) if all the dispersion were actually along the line of sight. If we assume Ursa Minor to be oblate rather than triaxial, and with the line of nodes in the plane of the sky, the dispersion we see is larger than one third of the total as we look along the major axis, implying an overestimate of the mass-to-light ratio. It is, however, likely that Ursa Minor is triaxial, a suggestion strengthened by the fact that it is possible to sustain rotation around the major axis of such a system. The effect of anisotropy in this case would be more difficult to calculate, as we do not know the size of the axis down which we are looking. Signs of triaxiality may be seen as the twisting of the surface-brightness isophotes and rotation of the apparent rotation axis with increasing radius. This anisotropy alone, however, cannot account for the large discrepancy between the mass-to-light ratio we have calculated for Ursa Minor and the values measured for larger and smaller stellar systems.

4.3.2 Binaries

The presence of binaries in the sample of observed stars would increase the observed velocity dispersion so that it was no longer a true indication of the mass of the galaxy. Suntzeff et al. (1993) made a calculation for Sextans using a Monte Carlo method. They obtained velocity dispersions of close to 6 km s^{-1} for a binary fraction of 0.25, assuming an intrinsic velocity dispersion of 2.1 km s^{-1}, which is equivalent to a mass-to-light ratio of 2.5 according to the parameters they used. Application of this same result to Ursa Minor merely implies that the starting mass-to-light ratio was 3, otherwise the result is the same. The calculation involved several simplifications, such as uniformity of mass ratios and inclinations and a flat period distribution, which are not necessarily valid, but it is still useful for comparison with the observations.

Aaronson & Olszewski (1988) have found three velocity variables among 18 stars in Ursa Minor. Two of these are likely to be variable because of motions in the atmospheres of the stars, but the other could well be a binary star. These results imply an observed binary fraction of between 0.06 and 0.17.

We have spectra at two epochs, separated by a year, for nine stars. For all these stars, the agreement between the velocities at the different epochs is almost within 2σ of the measuring errors; however, for two of these stars we only have one observation at each epoch and for none do we have as many as two observations at both epochs, which compares poorly with the equivalent data for Sextans, where we had two or three spectra at different epochs for several of the stars. Since for a binary fraction of 0.25 we would require only about two of these stars to be binaries, the result is inconclusive; although, with the velocities of five of our nine stars being within 1σ of the measuring errors, it is unlikely that the binary fraction as defined by Suntzeff et al. is much more than 25 per cent.

However, this is not the true picture because, due to our observing criteria, we can have detected only a fraction of the binary stars. Quantifying the possible binary fraction accurately requires continued velocity monitoring. Such efforts are important since a binary fraction of 0.1 still requires a true mass-to-light ratio of 50, whereas all extra

mass above that found in globular clusters can be explained by a fraction of 0.25.

4.3.3 *Tidal interaction with the Galaxy*

The other alternative is that the dSph galaxies are being tidally disrupted by the Milky Way Galaxy, so that the assumption of dynamical equilibrium underlying equations (3) and (4) is invalid. Tidal disruption caused by both the Galaxy and the Large Magellanic Cloud can account for much of the structure observed in the Small Magellanic Cloud, as well as the existence of the Magellanic Stream (Gardiner, Sawa & Fujimoto 1994). In addition, suggestive evidence for the existence of phase-space structure in the outer Galaxy, the reality of which would strongly support such a model of merging galaxies, continues to arise (Arnold & Gilmore 1992). Indeed, the concept of the small galaxies close to the Milky Way undergoing tidal disruption and merger is fundamental to standard cold dark matter cosmologies.

A completely disrupted dSph galaxy of freely expanding stars is expected to disperse in the time it takes for the galaxy to orbit our Galaxy, so that it is unlikely that a significant proportion of the nine known dSphs will be undergoing tidal disruption now. It is possible, however, that the dSph could still be visible as a collection of stars having been tidally disrupted some time ago, as shown by Kuhn (1993), who has performed *N*-body calculations demonstrating that, in the case of strong velocity anisotropy, the time for an unbound dSph galaxy to disperse may be an order of magnitude larger than a free expansion argument would suggest. If this were so, the velocity dispersion that we have been so diligently measuring would have nothing to do with the actual mass-to-light ratio of the galaxy.

For a mass-to-light ratio of 3, the mass of Ursa Minor would be $7.8 \times 10^5\ M_\odot$. Assuming this mass and a Keplerian potential for the Galaxy implies that the tidal distance of Ursa Minor is 104 kpc. This tidal distance is the distance at which a galaxy of a certain size and mass would have to be in order to be disrupted by the galaxy according to a simple balance of forces argument (Hargreaves et al. 1994). The actual distance of Ursa Minor is 64 kpc, indicating that Ursa Minor ought to be undergoing tidal disruption at present.

Calculations by Hodge & Michie (1969), and several numerical simulations since then, have suggested that a tidally disrupted satellite of the Galaxy ought to become elongated along the direction of its orbit. In the case of Ursa Minor, preliminary calculations of the proper motion indicate an orbit consistent with the direction of the Magellanic Stream (although the measuring errors here are large), and in the same orbital direction as the motion of the Large Magellanic Cloud (LMC) (Scholz & Irwin 1994). The major axis is within 10° of the direction of the likely orbital plane of the LMC, suggesting that Ursa Minor could have been elongated as predicted by the tidal disruption calculations. This, along with the discovery of structure in the luminosity contour map and the fact that Ursa Minor does have a profile indicative of truncation (Irwin & Hatzidimitriou 1994), adds evidence to the suggestion of tidal disruption.

A tidally disrupted dSph galaxy would become elongated along its orbit, losing stars because of frictional forces. Any stars on prograde orbits in the dSph galaxy would be expected to be preferentially lost. Therefore rotation in this direction may be lost as the dSph galaxy is disrupted, whereas the component of rotation in a direction perpendicular to the orbit of the dSph galaxy round the Galaxy would remain intact, eventually producing rotation only around the major axis, as we have found in Ursa Minor. In addition, it is possible to maintain rotation around the major axis in a triaxial system, suggesting that Ursa Minor is likely to be triaxial.

4.3.4 *Dark matter*

Should all the ideas in the previous sections fail to account for the high mass-to-light ratios, the alternative is that Ursa Minor contains large amounts of dark matter, with a core dark matter density of about $0.4\ M_\odot\ pc^{-3}$.

5 CONCLUSION

The internal central velocity dispersion of the Ursa Minor dSph galaxy is $7.5^{+1.0}_{-0.9}$ km s^{-1}, measured from 35 giant stars. There is rotation round the major axis with a gradient of $-4.7^{+2.0}_{-2.2}$ km s^{-1} per 100 pc, where positive distance is to the north-western side of the major axis. This leads to a corrected velocity dispersion of $6.7^{+0.9}_{-0.8}$ km s^{-1}. The mass-to-light ratios calculated using this value are 59^{+41}_{-25} and 40^{+29}_{-17} in solar units, using core-fitting and Illingworth's methods, respectively. By comparison, apparently purely stellar systems, such as globular clusters and the stellar Galactic disc, have mass-to-light ratios of about 3. Thus the observed internal velocity dispersion of the Sextans dSph galaxy is several times larger than the value of about 2 km s^{-1} that is expected if the galaxy is a self-gravitating stable system whose gravitational potential is dominated by the mass in visible stars.

There is, however, considerable evidence to indicate that things are not as simple as the mass-to-light ratio calculations assume. The discovery of rotation about the major axis, coupled with the evidence of structure in this dSph galaxy, is a clear indication of this. What exactly causes these effects is by no means as clear, but it is not unreasonable, given Ursa Minor's size and distance, that it should be undergoing tidal disruption, and we have suggested a possible explanation assuming this. This is that, as the dSph expands along the direction of its orbit, those stars that are causing the component of rotation round the axis perpendicular to the direction of motion are most likely to be lost, leaving only the other perpendicular component of rotation remaining. It is also possible that binary stars may be affecting the velocity dispersion, since binary fractions of only 0.25 can account for a dispersion of 6 km s^{-1}. With measurements at two dates, separated by about a year, for nine stars, the velocities for five of these were within 1σ of the measuring errors, the other four being within 2σ, so we have no firm identification of any binaries. However, we have too few observations at each epoch to say with any certainty that none of these stars is in a binary system. Further observations are required to ascertain the actual number of binaries in our sample of 35 stars.

Other possible explanations for our results include a substantial dark matter density in this Galaxy or a serious underestimate of the measuring errors. We think the latter unlikely. Another possible effect that may contribute is

velocity anisotropy, although it is unlikely to provide a major part of the answer.

ACKNOWLEDGMENTS

We thank E. W. Olszewski for giving us the positions of members of Ursa Minor found through his observations.

The spectroscopy reported here was obtained with the William Herschel Telescope operated on the island of La Palma by the Royal Greenwich Observatory in the Spanish Observatorio del Roque de los Muchachos of the Instituto de Astrofísica de las Canarias.

REFERENCES

Aaronson M., Olszewski E., 1987, in Kormendy J., Knapp G. R., eds, Proc. IAU Symp. 117, Dark Matter in the Universe. Reidel, Dordrecht, p. 153

Aaronson M., Olszewski E. W., 1988, in Audouze J., Pelleton M. C., Szalay A., eds, Proc. IAU Symp. 130, Large Scale Structure in the Universe. Reidel, Dordrecht, p. 409

Armandroff T. E., Da Costa G. S., 1986, AJ, 92, 777

Arnold R., Gilmore G., 1992, MNRAS, 257, 225

Cudworth K. M., Olszewski E. W., Schommer R. A., 1986, AJ, 92, 766

Fisher R. A., 1970, Statistical Methods for Research Workers. Oliver and Boyd, Edinburgh

Gardiner L. T., Sawa T., Fujimoto M., 1994, MNRAS, 266, 567

Gilmore G., 1990, in Lynden-Bell D., Gilmore G., eds, Baryonic Dark Matter. Kluwer, Dordrecht, p. 137

Hargreaves J. C., Gilmore G., Irwin, M. J., Carter D., 1994, MNRAS, 269, 957

Hodge P. W., Michie R. W., 1969, AJ, 74, 587

Irwin M. J., Hatzidimitriou D., 1993, in Smith G. H., Brodie J. P., eds, ASP Conf. Ser. Vol. 48, The Globular Cluster–Galaxy Connection. Astron. Soc. Pac., San Francisco, p. 322

King I., 1962, AJ, 67, 471

King I., 1966, AJ, 71, 64

Kuhn J. R., 1993, ApJ, 409, L13

Mateo M., 1994, in Meylan G., Prugniel P., eds, ESO/OHP Workshop on Dwarf Galaxies, p. 309

Mateo M., Olszewski E., Welch D. L., Fischer P., Kinkel W., 1991, AJ, 102, 914

Olszewski E. W., Aaronson M., 1985, AJ, 90, 2221

Paltoglou G., Freeman K. C., 1987, in de Zeeuw T., ed., Proc. IAU Symp. 127, Structure and Dynamics of Elliptical Galaxies. Reidel, Dordrecht, p. 447

Scholz R.-D., Irwin M. J., 1994, in MacGillivray H. T. et al., eds, Proc. IAU Symp. 161, Astronomy from Wide-Field Imaging. Kluwer, Dordrecht, p. 535

Suntzeff N. B., Mateo M., Terndrup D. M., Olszewski E. W., Geisler D., Weller W., 1993, ApJ, 418, 208

Tonry J., Davis M., 1979, AJ, 84, 1511

Zaritsky D., Olszewski E. W., Schommer R. A., Peterson R. C., Aaronson M., 1989, ApJ, 345, 759